

Atropisomerism and Conformational Equilibria: Impact on PI3K δ Inhibition of 2-((6-Amino-9H-purin-9-yl)methyl)-5-methyl-3-(*o*-tolyl)quinazolin-4(3H)-one (IC87114) and Its Conformationally Restricted Analogs

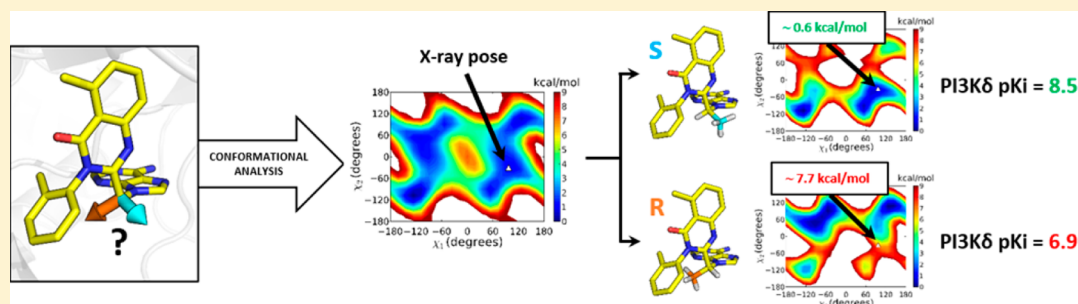
Alessio Lodola,[†] Serena Bertolini,[‡] Matteo Biagetti,[‡] Silvia Capacchi,[‡] Fabrizio Facchinetti,[‡] Paola Maria Gallo,[‡] Alice Pappani,[‡] Marco Mor,^{*,†} Daniele Pala,^{†,||} Silvia Rivara,[†] Filippo Visentini,[§] Mauro Corsi,[§] and Anna Maria Capelli^{*,‡}

[†]Dipartimento di Scienze degli Alimenti e del Farmaco, Università degli Studi di Parma, Viale delle Scienze 27/A, 43124 Parma, Italy

[‡]Chemistry Research and Drug Design Department, Chiesi Farmaceutici S.p.A., Largo F. Belloli 11/A, 43122 Parma, Italy

[§]Aptuit s.r.l., Via Fleming 4, 37135 Verona, Italy

Supporting Information



ABSTRACT: IC87114 [compound 1, (2-((6-amino-9H-purin-9-yl)methyl)-5-methyl-3-(*o*-tolyl)quinazolin-4(3H)-one)] is a potent PI3K inhibitor selective for the δ isoform. As predicted by molecular modeling calculations, rotation around the bond connecting the quinazolin-4(3H)-one nucleus to the *o*-tolyl is sterically hampered, which leads to separable conformers with axial chirality (i.e., atropisomers). After verifying that the aS and aR isomers of compound 1 do not interconvert in solution, we investigated how biological activity is influenced by axial chirality and conformational equilibrium. The aS and aR atropisomers of 1 were equally active in the PI3K δ assay. Conversely, the introduction of a methyl group at the methylene hinge connecting the 6-amino-9H-purin-9-yl pendant to the quinazolin-4(3H)-one nucleus of both aS and aR isomers of 1 had a critical effect on the inhibitory activity, indicating that modulation of the conformational space accessible for the two bonds departing from the central methylene considerably affects the binding of compound 1 analogues to PI3K δ enzyme.

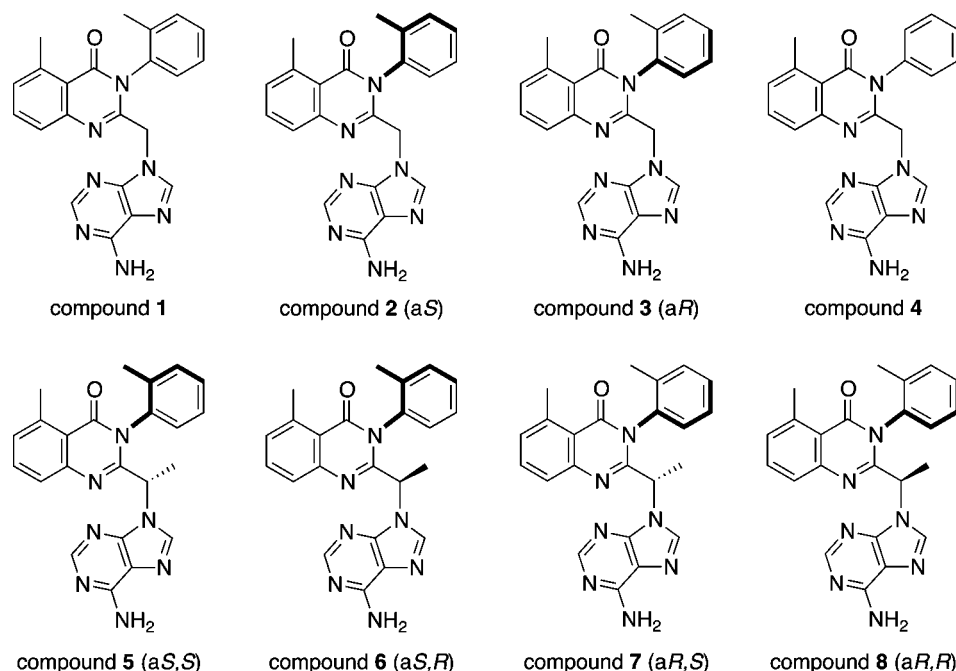
INTRODUCTION

Atropisomerism is a source of molecular asymmetry arising from the presence of a restricted rotation along a covalent bond in a given structure, giving rise to stable conformers with axial chirality (atropisomers) that can be isolated as distinct chemical species when their interconversion half-life is sufficiently long, e.g., higher than 1000 s.¹ Drugs containing classical stereogenic centers are considered stable compounds as they can only racemize through bond breaking processes. Conversely, atropisomers racemize through a simple bond rotation with a time scale ranging from minutes to years, depending on steric hindrance, electronic factors, temperature, and solvent. Atropisomeric compounds, like classical enantiomers, are featured by different pharmacodynamics and pharmacokinetics profiles.^{2,3} Indeed, for several atropisomer pairs, significant variation in in vitro inhibition or binding data⁴ as well as in ADMET properties⁵ have been reported in the literature.^{6,7}

The decision to develop a drug candidate as an atropisomer should be in place as early as possible during the lead optimization stage as the existence of multiple atropisomers would even further complicate their drug development in terms of stability on the shelf and potential risk of interconversion after administration. Despite these critical issues, no direct guidelines as to how deal with time-dependent chirality have been delivered by regulatory agencies.⁸ On the other hand, pharmaceutical companies have developed theoretical and experimental protocols to characterize atropisomer interconversion in order to facilitate well-versed decisions about storage and handling of compound under pharmaceutical development.^{9,10}

Received: February 14, 2017

Published: May 10, 2017

Chart 1. Chemical Structures of PI3K δ Inhibitors Considered in This Study

We recently focused our attention on 2-((6-amino-9H-purin-9-yl)methyl)-5-methyl-3-(*o*-tolyl)quinazolin-4(3H)-one, (IC87114, compound 1, Chart 1), a potent and selective inhibitor of the phosphoinositide 3-kinase (PI3K) δ isoform,¹¹ an enzyme that has been implicated in several pathological conditions, including autoimmune and inflammatory diseases and B-cell malignancies. Since compound 1 has been widely utilized as tool compound to carry out both in vitro and in vivo experimental studies on PI3K δ , its in-depth characterization may help to better interpret the data generated so far.

For this derivative, the rotation along the bond connecting the quinazolin-4-one moiety to the *N*-tolyl fragment appears to be hindered, suggesting that 1 may exist as a mixture of two separable atropisomers, i.e., the aS isomer, where the methyl group of the tolyl group lies above the plane of the quinazolin-4-one ring (Chart 1, compound 2), and the aR isomer (Chart 1, compound 3), where the methyl group lies on the opposite side of that plane.

In fact, a patent application¹² describes a method to obtain, by chiral chromatography, the two optically active atropo-enantiomers 2 and 3, reporting similar IC₅₀ values for PI3K δ inhibition and different pharmacokinetics. In the same patent, the first eluting compound was identified as the aS atropisomer 2 by X-ray diffraction. Prompted by this report, we decided to explore the composition of the commercial batches of 1, predict and measure the stability of each atropisomer, and investigate the influence of steric effects related to the conformational space of 1 on PI3K δ inhibitor potency.

Although compound 1 is regarded as one of the reference inhibitors of PI3K δ enzyme, for which several bioanalytical methods have been recently validated to determine its plasmatic level in mice,^{13,14} no data about its axial chirality are provided for commercial batches. As atropisomerism often goes both undetected and unsuspected given that enantiomers cannot be distinguished using routine analytical tools (¹H NMR, HPLC, etc.),^{8,9} it might be the case that the compound employed for biological tests is actually a racemic mixture of

atropisomers. Our work started with the characterization of a commercial batch of 1, isolation of atropo-enantiomers, and their identification by vibrational circular dichroism (VCD). The extent of mutual conversion of 2 and 3 was measured at conventional temperatures to assess the risk that, starting from an atropo-enantiomer, racemization could occur during compound manipulation and biological tests.

Atropisomerism is a particular feature of conformational space, where energetic barriers are too high to be freely crossed at room temperature. While equilibria among conformations separated by low energy barriers can be investigated by free-energy calculations employing molecular mechanics force fields, higher barriers, like those involved in atropisomerism, require contributions from quantum mechanics (QM).^{8,9} Estimation of the barrier for rotation about the bond involved in axial chirality was qualitatively compared to stability data to confirm the predictive ability of QM-based computational protocols.

In a more general sense, equilibria among accessible conformations of a drug can affect its propensity to interact with specific targets, and the ability to predict the effect of chemical modifications on biological properties is essential to drug design and development. Applications of computational protocols to the study of the conformational space of drugs and investigations on its relevance for drug–protein interactions have been reported in the literature.^{15,16} Available information about the inhibitor mechanism of 1 on PI3K δ suggests that reciprocal arrangements of the tolylquinazolinone and adenyl moieties are essential for binding at the active site.¹⁷ Thus, we combined computational and experimental techniques to explore in a wider sense the relationship between the conformational space of compound 1, with its close derivatives, and affinity for PI3K δ . The conformational free-energy surface (FES) of a bioactive compound provides critical information for drug design purposes. Knowledge of the penalty (i.e., strain-energy, ΔE_{strain}) that a ligand has to pay for leaving the global-minimum basin in solution and adopting the target-binding conformation¹⁸ is instrumental to design conformationally

restricted compounds exhibiting smaller ΔE_{strain} , hence expected to be more potent than their flexible analogues.

The X-ray crystal structure of a rotamer, corresponding to the putative aS atropisomer of **1** (i.e., compound **2**), bound to the catalytic domain of human PI3K δ (PDB code 2X38)¹⁷ shows that the adenine moiety of this ligand takes hydrogen-bond interactions with the hinge amino acids, whereas the quinazolinone fragment is accommodated in the “specificity pocket” beneath the enzyme P-loop. The tolyl group is located at the entrance of the cavity where the binding pocket is wide and solvent exposed (Figure 1).¹⁷

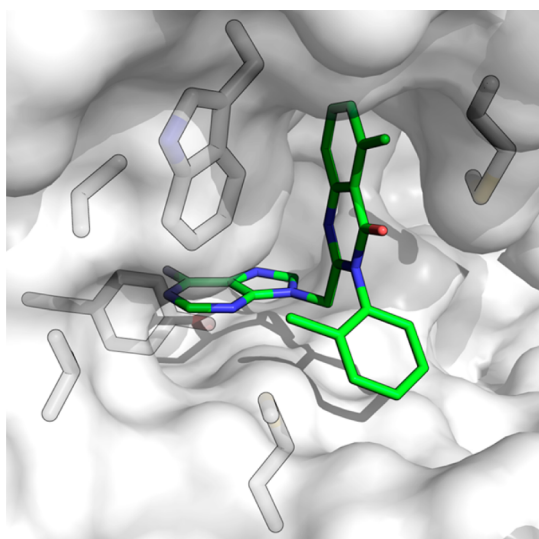


Figure 1. aS atropisomer of **1** (compound **2**, green carbon atoms) in complex with PI3K δ (white carbon atoms) as revealed by X-ray crystallography (PDB code 2X38).¹⁷

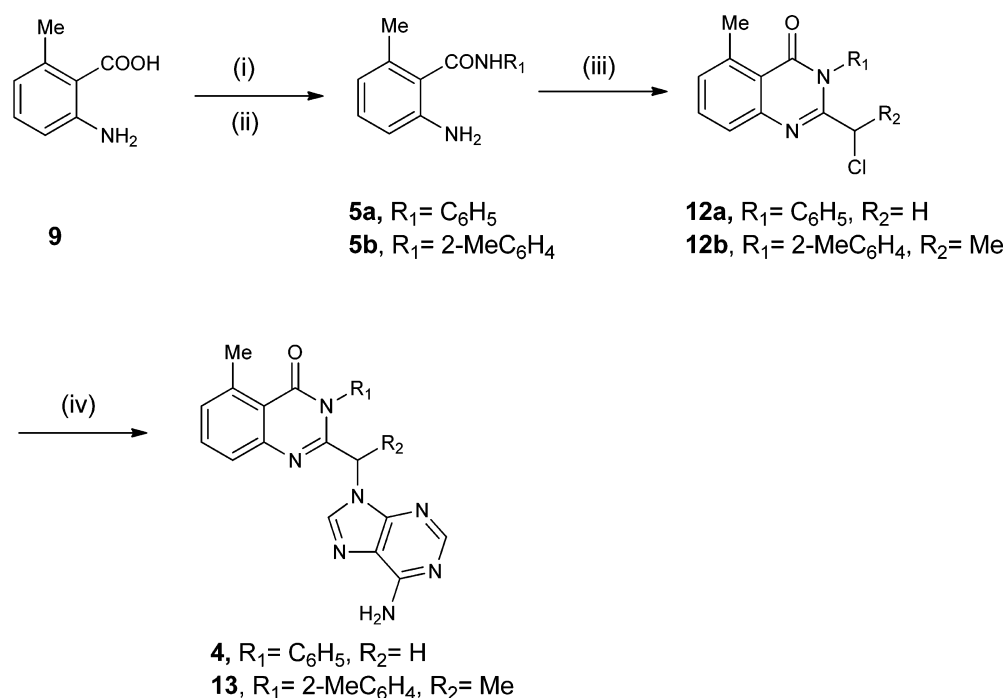
Visual inspection of this complex and molecular docking (not shown) suggest that the rotamer with opposite orientation of the tolyl fragment (corresponding to the putative aR atropisomer, structure **3**) can also be accommodated into the ATP-binding site of PI3K δ . While the absence of atropo-stereoselectivity can be anticipated by similar potency data reported for the two atropisomers in the cited patent, we speculated that modulation of the conformational space accessible for the two bonds departing from the central methylene could affect binding site activity. In particular, the introduction of a methyl group on the methylene spacer connecting the adenine ring to the quinazolinone nucleus of **2** and **3** (leading to the atropodiastereoisomer couples **5–6** and **7–8**) could restrict the conformational space of these compounds compared to that of the reference inhibitor **1** and thus affect their inhibitory potency. Hence, an investigation of the conformational space of compound **2** and its analogues together with the assessment of their biological profile appears fundamental to evaluate the impact of atropisomerism and conformational equilibria on PI3K δ inhibition.

Here we report the characterization of compound **1** as an atropisomeric mixture, the isolation of pure aS and aR atropisomers followed by their extensive characterization in terms of stability, conformational preferences, and biological profile. Finally, a few conformationally restricted analogues characterized by the presence of both axial chirality and stereogenic centers were in depth investigated.

RESULTS AND DISCUSSION

Chemistry. Compound **1** was purchased from Symansis, while single atropisomers (compound **2** and compound **3**) were obtained from HPLC separation of the racemate (see [Experimental Section](#) for details). The preparation of

Chart 2. Synthesis of Compound **4** and the Racemic **13**^a



^aReagents and conditions: (i) SOCl_2 (3.0 equiv), toluene, 18 h, reflux; (ii) $R_1\text{NH}_2$ (1.5 equiv), TEA (1.5 equiv), DCM, 2 h, reflux; (iii) $\text{Cl-CHR}_2\text{COCl}$ (**11a**, $R_1 = \text{H}$; **11b**, $R_1 = \text{Me}$), AcOH, reflux, 18 h; (iv) adenine (1.5 equiv), K_2CO_3 (1.5 equiv), acetonitrile.

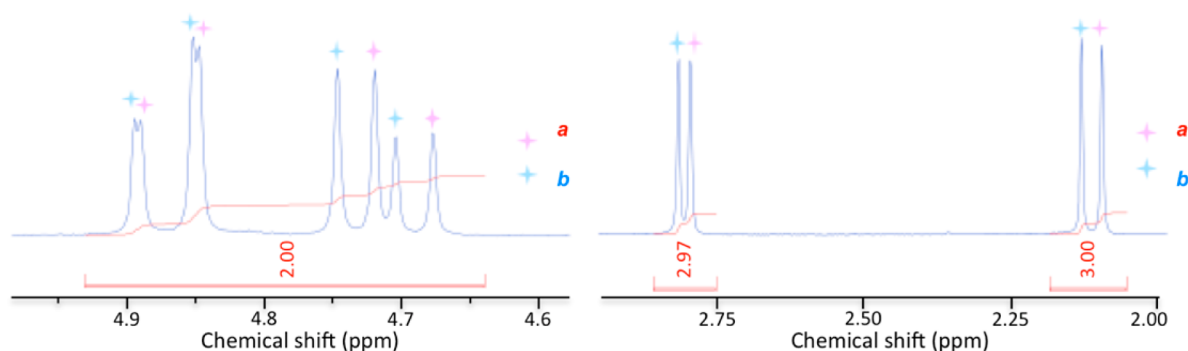


Figure 2. Left: Splitting of CH_2 signals observed in the ^1H NMR spectra of the association complex 1:R-Pirkle. Right: Splitting of signals observed in the ^1H NMR spectra of the association complex 1:R-Pirkle for the two methyl groups on the quinazolinone nucleus (2.8 ppm) and on the phenyl ring (2.1 ppm). Letters *a* and *b* indicate the two atropisomers.

quinazolinone analogues of **1**, namely, compound **4** and the racemic mixture **13**, was carried out according to the procedure described in Chart 2. In particular, 2-amino-6-methylbenzoic acid **9** was converted into the corresponding acid chloride by reaction with SOCl_2 and then reacted with the suitable anilines to afford amides **10a,b**. Quinazolinone scaffolds **12a,b** were then built up by further reaction of **10a,b** with a 2-chloroacetyl chloride derivatives **11a,b** in refluxing acetic acid. Chlorides **12a,b** were finally reacted with adenine in the presence of K_2CO_3 to afford **4** and racemic **13**. Single diastereoisomers **5–8** were isolated from **13** by preparative chiral HPLC using a Chiralpak IA column (see Experimental Section for details).

Spectroscopic Characterization of Compound 1. First of all, we investigated whether a commercial batch of compound **1** consists of an achiral compound with free rotation of the tolyl fragment, an optically pure atropisomer, or a mixture of both atropisomers. For this purpose, compound **1** purchased from Symansis was fully characterized in CDCl_3 by means of NMR experiments. The 1D NMR spectrum confirmed the proposed structure for **1** (Supporting Information, Figure S1). As ^1H NMR cannot detect the existence of mirror-image enantiomers, the chiral reagent (1*R*)-1-(anthracen-9-yl)-2,2,2-trifluoroethanol (*R*-Pirkle) was used to generate diastereoisomeric complexes with compound **1** in solution. This approach allowed identification enhanced shift effects resulting from the formation of hydrogen bonds between the ligand and the chiral reagent. Shift effects were detected using a 1:10 molar ratio (Figure S2). In particular, splitting of signals for the methylene group connecting the two moieties and for the two methyl groups on the quinazolinone nucleus and on the phenyl ring were clearly observed (Figure 2), consistent with the presence of two atropodiastereoisomers in solution, indicating that the commercial batch of compound **1** is indeed a mixture of the *aS* (**2**) and *aR* (**3**) atropisomers.

Separation and Characterization of Atropisomers 2 and 3. The existence of atropisomer chirality for **1** was also confirmed by HPLC on a chiral support, which shows the existence of two distinct peaks (A and B). The first eluting atropisomer [peak A, (–) compound] possesses the *aS* chiral center (i.e., compound **2**, Chart 1), while the second eluting atropisomer [peak B, (+) compound **3**, Chart 1] had an *aR* chiral center, as deduced by vibrational circular dichroism (VCD) analysis in combination with density functional theory (DFT) calculations¹⁹ (see Experimental Section for details). Having isolated and identified the structure of atropisomers **2** and **3**, we next evaluated their thermal interconversion in dimethyl sulfoxide (DMSO) at two different temperatures and

two concentrations by chiral HPLC/MS. At $-20\text{ }^\circ\text{C}$, no racemization was observed for either compound **2** or compound **3** (data not shown). At $37\text{ }^\circ\text{C}$ (Figure 3), both

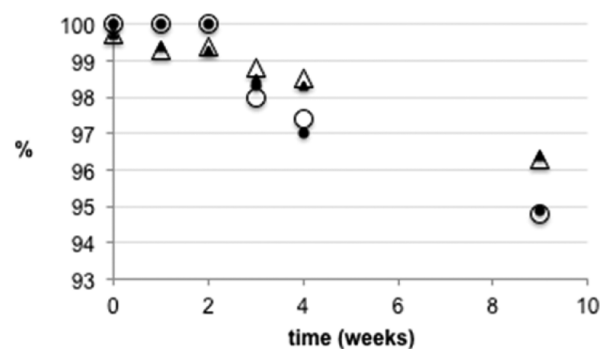


Figure 3. Time course of reciprocal conversion of **2** (circles) to **3** (triangles) in dimethyl sulfoxide (DMSO), starting from concentrations of 1 mM (hollow) or 10 mM (filled). Percentages of original atropisomer found in DMSO solution are reported as a function of time.

compound **2** and compound **3** underwent a slow racemization process, with nearly a 5% of conversion after 9 weeks of incubation in solution, irrespective of the starting concentration of the sample.

Altogether, these findings confirm that compound **2** and compound **3** can be isolated as optically pure compounds and that their stability is sufficient for further investigations on single atropisomers.

Calculation of Atropisomer Interconversion Barrier.

The finding that compounds **2** and **3** showed a slow but observable racemization in solution of dimethyl sulfoxide (DMSO) prompted us to estimate the rate of atropisomer conversion by means of computational methods. To this end, we calculated the torsional energy barrier around the bond connecting the quinazolin-4-one moiety with the ortho-tolyl fragment in gas phase by means of quantum mechanics (QM) and in explicit solvent using a hybrid quantum mechanics/molecular mechanics (QM/MM) approach.²⁰ The use of a QM-based potential is necessary to obtain information about the energy of the transition state (TS) separating the two stable atropisomers. As classical force fields are not expected to give robust energetic estimates for TS configurations unless they are specifically parametrized for this purpose,²¹ DFT-based approaches²² were used to generate TS structures and

subsequently to calculate the barrier for atropisomer conversion.

At first, the relationship between the potential energy and the rotation around the ϕ dihedral angle in 2,5-dimethyl-3-(*o*-tolyl)quinazolin-4(3*H*)-one, a simplified model of compound 2 (Figure 4), was assessed with the use of B3LYP hybrid functional²³ and the 6-31G* basis set.

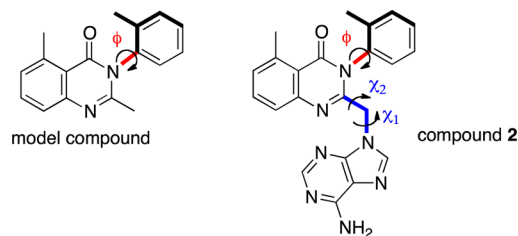


Figure 4. Chemical formulas of the compounds employed in the calculation of the rotational barrier around the ϕ dihedral angle (depicted in red) by QM or QM/MM methods or for exploration of the free-energy surface around χ_1 and χ_2 dihedral angles (depicted in blue) by *wt*-metadynamics.

In the first torsional scan, rotation of the ϕ dihedral angle was performed from 90° to -90° , with 0° corresponding to the eclipsed conformation having the methyl group in contact with the carbonyl oxygen. The ϕ angle was set to different values, and a constrained geometry optimization was performed at B3LYP/6-31G* level. The potential energy values thus obtained are represented in Figure 5. On the basis of the line connecting these values, the potential energy of atropisomer conversion amounted to 28.0 kcal/mol.

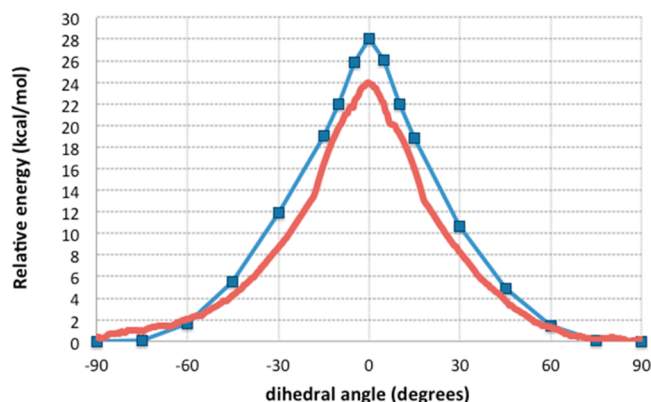


Figure 5. Potential energy profile (blue line) in gas phase along the dihedral angle ϕ for the model compound at B3LYP/6-31G* level and free-energy profile (red line) in explicit water along the same dihedral angle for compound 2 at SCC-DFTB/AMBER level of theory.

The rotation of the same dihedral angle from -90° to 180° (i.e., with the two methyl groups approaching each other) gave higher energy values due to unfavorable steric interactions of the methyl group of the tolyl substituent with the 2-methyl group of the quinazolin-4-one scaffold (data not shown). This is consistent with the results of recently reported calculations¹⁰ and points out that the passage of the ortho-methyl over the carbonyl oxygen is more likely to occur during atropisomer interconversion. Subsequently, we calculated the free energy of atropisomer conversion for compound 2 in explicit water, using a hybrid QM/MM potential (SCC-DFTB/AMBER)^{24,25} and

applying an umbrella-sampling approach.²⁶ Also in this case, the conformational sampling around the bond connecting the quinazolin-4-one moiety with the ortho-tolyl one was performed from 90° to -90° . The shape of the resulting free energy curve was similar to that calculated in gas phase for model compound (Figure 5), whereas the free-energy barrier for the conversion of 2 in 3 was 24.0 kcal/mol.

As SCC-DFTB is a semiempirical method known to underestimate energy barriers,²² the free energies of the approximate transition state and of the reactant were corrected at B3LYP/6-31G* level (see Experimental Section for details). The corrected B3LYP/6-31G*//SCC-DFTB/AMBER free-energy barrier was as high as 28.5 kcal/mol, very similar to that found for the model compound in gas phase (28.0 kcal/mol) and for similar quinazolinone inhibitors of PI3K δ recently reported in the literature.²⁷ Thus, the rate of atropisomer conversion seemed to primarily depend on the steric repulsion between the quinazolin-4-one oxygen and the ortho-methyl group of the tolyl fragment, whereas solvation and entropic effects played a negligible role. The calculated barrier of 28.5 kcal/mol corresponds to a half-relaxation time for racemization of nearly 90 days at 37°C (deduced from the Eyring equation),²⁸ suggesting that compounds 2 and 3 can be isolated and tested in vitro without racemization, in agreement with results obtained from stability studies. According to the classification system of atropisomers,⁸ compound 2 belongs to class 2 as it experiences delayed axial interconversion, with a half-relaxation time greater than hours.

Conformational Analyses of Compound 1 Derivatives by Well-Tempered Metadynamics. We continued our computational investigation on the conformational preferences displayed by compound 2 by characterizing its conformational FES in explicit solvent with the use of a well-tempered metadynamics (*wt*-META-D) approach²⁹ and OPLS2005 force field.³⁰ To this end, the two dihedral angles χ_1 and χ_2 , describing the possible orientations of the adenine ring with respect to the quinazolin-4-one nucleus (Figure 4), were employed as collective variables during a 50 ns long *wt*-META-D simulation (see Experimental Section for details). Different from molecular dynamics (MD) requiring long simulation time to evaluate conformational changes, META-D has emerged as a fast, robust, and efficient tool to evaluate free energy changes of solvated systems.³¹ This approach is an artificial MD simulation in which the evolution of the system is biased by a history-dependent potential constructed as a sum of Gaussian functions centered along a set of collective variables (CVs), which are assumed to provide a description of the desired conformational transformation.³² The added Gaussians allow the system to escape from local minima³³ and are fundamental to reconstruct the conformational free energy surface (FES).³⁴

The resulting two-dimensional FES (Figure 6) shows the presence of six distinct basins (A–F) corresponding to specific conformations of compound 2. All these minima are featured by a comparable free energy and therefore similarly populated in solution. Calculations also showed that the conformation assumed by compound 2 in the complex with PI3K δ enzyme ($\chi_1 = 97^\circ$ and $\chi_2 = -30^\circ$, as obtained from the X-ray structure depicted in Figure 1) corresponds to a well-defined free-energy minimum (basin E). This finding suggests the accommodation of 2 within PI3K δ is driven by conformational selection; i.e., compound 2 is not forced into a high-energy state by the ATP binding site of the enzyme.

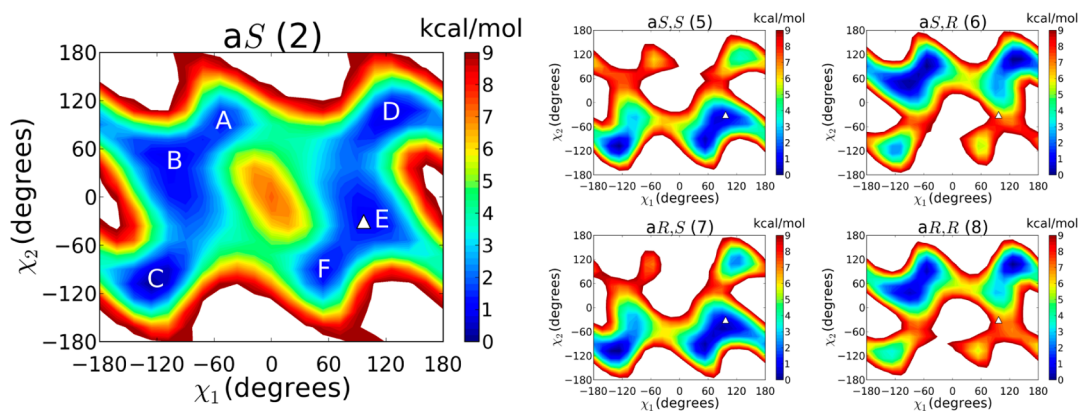


Figure 6. Two-dimensional plot of the conformational free energy surface of **2** (left panel) and **5–8** (right panels) in water constructed in the χ_1 and χ_2 space from 50 ns long *wt*-META-D using OPLS-2005 force field. The contours are drawn at 1 kcal/mol. The triangle indicates χ_1 and χ_2 values observed for compound **2** in the X-ray complex with PI3K δ enzyme.

Subsequently, we investigated the conformational preferences of the diastereomeric couple formed by compounds **5** and **6** that, in addition to the *aS* chiral axis, also possess an *S* or an *R* chiral center, respectively. Both compounds were submitted to *wt*-META-D simulations in explicit water employing the same computational protocol used for **2**. The resulting FESs are also reported in Figure 6. In both cases, the introduction of a methyl group on the hinge methylene connecting the adenine ring to the quinazolin-4-one nucleus drastically affects the energetics of the conformational space along χ_1 and χ_2 compared to the parent compound **2**. In the case of the *aS*, *S* isomer (compound **5**), A, B, and D free-energy areas become low-populated states being separated by the global minimum C of nearly 4 kcal/mol in case of D and more than 7 kcal/mol in the cases of A and B. Conversely, basin E (corresponding to the bioactive conformation of **2**) remained an accessible conformational state being higher than C by less than 1 kcal/mol. In the case of the *aS*, *R* isomer (compound **6**), we obtained a specular FES, i.e., with basin D as a global minimum and C, E, and F regions as high free-energy areas, separated from the former minimum by approximately 3, 8, and 6 kcal/mol.

Similar FESs were obtained when the *wt*-META-D simulations were performed for the *aR*, *S* (compound **7**) and *aR*, *R* (compound **8**) diastereomeric pair (Figure 6), confirming that the conformational space of these derivatives is driven primarily by the spatial orientation of the newly introduced methyl group, whereas the chiral axis lying on the ϕ dihedral has a limited effect on the conformational free energy of the identified basins. It is important to point out that the conformational free-energy differences estimated for compounds **2**, **5–8** by *wt*-META-D refer to simulations that reached convergence (see Experimental Section for details and Figures S3–S7). *wt*-META-D simulations were replicated for compounds **2**, **5**, and **6** applying different starting velocities, similar to those reported in ref 35. No significant changes were observed in the computed FESs calculated in three replicas (Figure S8).

While the FESs point out that the lower inhibitor potency of compound **6** with respect to its diastereoisomer **5** can be attributed to an energy strain, resulting from lower abundance of the active conformation, the difference of the free energy calculated by metadynamics (approximately 7 kcal/mol) appears to be overestimated. This may be due to the low accuracy of the force-field functions when dealing with nonminimum energy geometries. To get a more accurate

evaluation of conformational energies, the geometries of OPLS-2005 minima identified with the META-D protocol were optimized at DFT level using the M06-2X density functional.³⁶ Geometry optimization (energy minimization with 6-31G** basis set) were performed in implicit water, and the resulting structures were utilized for single point energy calculations with a larger basis set, cc-PVTZ(-f), using the same density functional and solvation model. Considering that compounds **5** and **6** are enantiomers of compounds **8** and **7**, respectively, we limited these calculations to compounds **2**, **5**, and **6**. M06-2X/cc-PVTZ(-f) energies calculated for conformers A–F of compounds **2**, **5**, and **6** are reported in Table S1 of the Supporting Information. For compound **2**, the energy difference between the minimum-energy conformation (conformer A of the FES) and the PI3K δ -binding minimum is 2.4 kcal/mol, suggesting that its accommodation into the PI3K δ binding site involves significant strain (ΔE_{strain}). As for compound **5**, the ΔE_{strain} value is slightly smaller (1.7 kcal/mol), whereas for compound **6** it increases up to 3.7 kcal/mol. The calculated energy penalties for reaching the binding conformation mirror the difference in inhibitory potency at PI3K δ enzyme.

Biological Evaluation. Following these extensive analytical and computational analyses, compounds **2** and **3** were next tested for their ability to inhibit recombinant PI3K δ enzyme and to block the release of the inflammatory mediator interleukin-6 (IL-6) from human peripheral blood mononuclear cells (PBMCs).³⁷ As shown in Table 1, compounds **2** and **3** have comparable potency in both these assays, indicating that the orientation of the ortho-tolyl fragment is not relevant for binding to the enzyme. This is in line with the visual inspection of the crystal structure of the PI3K δ -**2** complex showing that compound **3** could similarly fit the ATP-binding site of the enzyme. This conclusion was further confirmed by compound **4**, which lacks atropisomerism and exhibited a biological profile similar to those of compounds **2** and **3**.

On the contrary, the spatial orientation of the methyl group introduced on the hinge connecting adenine and quinazolin-4-one moieties considerably affects the inhibitory potency of the synthesized atropo diastereomers **5–8**. The *aS*, *S* isomer **5** was considerably more potent than the *aS*, *R* isomer **6** which registered a 30-fold drop in the inhibitory activity on PI3K δ enzyme. Similar findings were obtained comparing the activity of the *aR*, *S* isomer (**7**) with the *aR*, *R* one (**8**), with the former being nearly 10-fold more potent than the latter.

Table 1. Potency Values on Recombinant Human PI3K δ (Expressed as pK $_i$ Values) and on Interleukin-6 (IL-6) Release from Human Blood Mononuclear Cells (Expressed as pIC $_{50}$ Values) for Compounds 2–8

compd	chirality ^a	PI3K δ , pK $_i$ ^b	IL-6 release, pIC $_{50}$ ^c
2	aS	7.9 \pm 0.03	7.6 \pm 0.1
3	aR	7.7 \pm 0.1	7.3 \pm 0.1
4		7.6 \pm 0.1	7.3 \pm 0.4
5	aS, S	8.5 \pm 0.1	8.2 \pm 0.5
6	aS, R	6.9 \pm 0.04	NT ^d
7	aR, S	8.8 \pm 0.1	8.9 \pm 0.1
8	aR, R	7.9 \pm 0.03	NT ^d

^aChirality was determined with vibrational circular dichroism (VCD; see [Experimental Section](#) for details). ^bpK $_i$ values were obtained with Cheng and Prusoff equation from experimental IC $_{50}$ values and are the mean \pm SD of four determinations performed in duplicate. ^cpIC $_{50}$ values are the mean \pm SD of two independent determinations performed in quadruplicate. ^dNot tested.

Visual inspection of the PI3K δ –2 complex ([Figure 1](#)) suggests that the introduction of a small group on the methylene hinge of 2 should not affect the inhibitory potency of the class, as both the pro-*S* and pro-*R* hydrogens of this methylene point toward an empty region of the ATP binding site of PI3K δ . On the basis of the simulations reported above, we propose that compound 5 inhibits PI3K δ more efficiently than 6 because it can easily adopt the conformation assumed by the reference inhibitor 2 in the crystal structure with PI3K δ ([Figure 7a](#)), while compound 6 can assume the bioactive

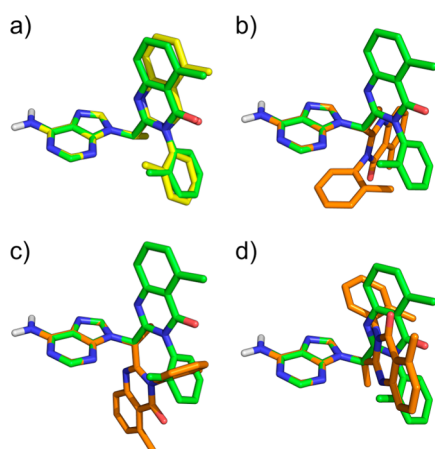


Figure 7. (a) Superposition of a minimum free-energy conformation of compound 5 (yellow carbon atoms, taken from energy basin E of [Figure 6](#)) on the bioactive one assumed by compound 2 (green carbon atoms) in its crystallographic complex with PI3K δ enzyme. (b–d) Superposition of highly populated free-energy conformations of compound 6 (orange carbon atoms, taken from basins A, B, and D of [Figure 6](#)) on the bioactive conformation of compound 2 (green carbon atoms).

conformation only paying a free-energy penalty. Moreover, not one of the other accessible conformations identified for 6 (i.e., lying on basins A, B, and D of [Figure 6](#)) is able to fit the pharmacophore elements possessed by compound 2 in its complex with PI3K δ as indicated by the superpositions reported in [Figure 7b–d](#).

CONCLUSIONS

Atropisomerism is the drug chirality due to slowly interconverting compound conformations as a result of either steric or electronic hindrance allowing their isolation. Compounds exhibiting this chirality can have different efficacy, selectivity, and pharmacokinetic profile similar to enantiomers. Even though recent literature has contributed to increase the awareness of their potential issues, they are frequently overlooked in medicinal chemistry projects. Besides, the lack of clear guidance from the regulatory agencies further complicates this scenario.

Here we have demonstrated with the use of NMR chiral reagents that compound 1, a standard PI3K δ inhibitor extensively used to carry out in vitro and in vivo experiments for this enzyme, is a mixture of atropisomers. Besides, we have shown by using HPLC that at 37 °C they undergo a very slow racemization process, consistent with their calculated free energy conversion of 28.5 kcal/mol in explicit water so that they can be separated and characterized. The QM/MM calculations have shown that the rate of atropisomer conversion mainly depends on the steric repulsion between the quinazolin-4-one oxygen and the ortho-methyl group, whereas solvation and entropic effects seem to be negligible.

The introduction of a stereogenic center on top of the axial chirality changes the biological profiles of the diastereoisomers obtained. In particular, the *S* stereogenic center increases both the enzymatic and the cell-based potency inhibition with respect to the *R* one. Besides, the combination of the *S* stereogenic center with the aS chirality provides the most potent compound. This is also the only derivative out of the four diastereoisomers showing that the bioactive conformation observed in the crystal structure is energetically accessible.

EXPERIMENTAL SECTION

Chemical Synthesis. General Methods. All reactions were carried out under argon atmosphere. Solvents were purchased from commercial sources and used without further drying: ammonium formate for HPLC, $\geq 99.0\%$ (Fluka); acetonitrile LC–MS Ultra CHROMASOLV tested for UHPLC–MS (Fluka); methanol LC–MS Ultra CHROMASOLV tested for UHPLC–MS (Fluka).

Compound 1 (2-((6-amino-9*H*-purin-9-yl)methyl)-5-methyl-3-(*o*-tolyl)quinazolin-4(3*H*)-one) was purchased from Symansis (www.symansis.com). Chiral reagent (1*R*)-1-(anthracen-9-yl)-2,2,2-trifluoroethanol (*R*-Pirkle) was purchased from Sigma. Solvents DMSO-*d*₆ and CDCl₃ were 99.96% pure and were purchased from Merck. Silica gel chromatography purifications were performed in flash conditions using either glass columns packed with 230–400 mesh silica gel (Merck) or prepacked silica gel cartridges (Biotage). Analytical thin layer chromatography (TLC) was carried out on Merck silica gel plates (silica gel 60 F254). ¹H NMR and ¹³C NMR spectra were recorded on a Bruker Avance 200 spectrometer, using CDCl₃ or DMSO-*d*₆ as solvent. Chemical shifts (δ scale) are reported in parts per million (ppm) relative to the central peak of the solvent. Coupling constants (*J* values) are given in hertz (Hz). EI-MS spectra (70 eV) were taken on a Fison Trio 1000; molecular ions (M⁺ or M[−]) are given. ESI-MS spectra were taken on a Waters Micromass ZQ instrument; only molecular ions (M + 1 or M − 1) are given. Melting points were determined on a Buchi SMP-510 capillary melting point apparatus and are uncorrected. Microwave reactions were carried out using Biotage Initiator microwave synthesizer. Specific rotations were measured on a Bellingham Stanley ADP440+ polarimeter. The purity of the compounds reported in the manuscript was established through HPLC methodology, with both UV and MS detection. All the tested compounds reported in the manuscript have a chemical purity greater than 95%.

(*aS*)-2-[(6-Amino-9H-purin-9-yl)methyl]-5-methyl-3-(2-methylphenyl)quinazolin-4(3H)-one (**2**). IC78114 was separated by preparative chiral HPLC on a Chiralpak IA under isocratic elution at 60 mL/min eluting with DCM + 0.1% diethylamine to give as first eluting isomer **2** ($t_R = 10.9$ min). MS (ESI): 398.1 $[M + H]^+$; $[\alpha]_D^{20} +40.6$ (c 2.4, $CHCl_3$). 1H NMR (400 MHz, $DMSO-d_6$): δ ppm 2.18 (s, 3 H), 2.73 (s, 3 H), 4.56–5.23 (m, 2 H), 7.07–7.25 (m, 3 H), 7.30 (d, 1 H, $J = 7.1$ Hz), 7.39–7.54 (m, 4 H), 7.61 (t, 1 H, $J = 7.9$ Hz), 8.05 (d, 2 H, $J = 4.4$ Hz).

(*aR*)-2-[(6-Amino-9H-purin-9-yl)methyl]-5-methyl-3-(2-methylphenyl)quinazolin-4(3H)-one (**3**). Starting from the commercial bath of compound **1**, atropisomer **3** was recovered as second eluting compound ($t_R = 12.8$ min) in the same chromatographic run employed to isolate **2**. MS (ESI): 398.1 $[M + H]^+$; $[\alpha]_D^{20} -39.7$ (c 2.6, $CHCl_3$). 1H NMR (400 MHz, $DMSO-d_6$): δ 2.18 (s, 3 H), 2.73 (s, 3 H), 4.56–5.23 (m, 2 H), 7.07–7.25 (m, 3 H), 7.30 (d, 1 H, $J = 7.1$ Hz), 7.39–7.54 (m, 4 H), 7.61 (t, 1 H, $J = 7.9$ Hz), 8.05 (d, 2 H, $J = 4.4$ Hz).

2-[(6-Amino-9H-purin-9-yl)methyl]-5-methyl-3-phenylquinazolin-4(3H)-one (**4**). 2-(Chloromethyl)-5-methyl-3-phenylquinazolin-4(3H)-one **12b** (0.052 g, 0.183 mmol) was dissolved in acetonitrile (10 mL) and few drops of DMF. K_2CO_3 (0.038 g, 0.274 mmol) and adenine (0.037 g, 0.274 mmol) were added, and the mixture was reacted at 65 °C for 6 h. Acetonitrile was removed under reduced pressure, and the suspension was poured into water (30 mL) and stirred at room temperature for 30 min and then cooled to 5 °C. The solid was filtered and dried and the resulting material was purified by silica gel flash chromatography with a gradient of DCM and MeOH to give the title compound **4** (0.037 g, 0.097 mmol, 53% yield). MS (ESI): $[M + H]^+ 313.2$. 1H NMR (300 MHz, $DMSO-d_6$): δ 7.98–8.11 (m, 2 H), 7.41–7.69 (m, 3 H), 7.19–7.33 (m, 2 H), 7.10–7.18 (m, 1 H), 5.00 (s, 2 H), 2.73 (s, 3 H).

(*aS,S*)-2-[(6-Amino-9H-purin-9-yl)methyl]-5-methyl-3-phenylquinazolin-4(3H)-one (**5**). Mixture of diastereoisomers **13** was separated by chiral HPLC on a Chiralpak IC under isocratic elution at 0.8 mL/min (phase A/B = 65/35% v/v; phase A, hexane; phase B, EtOH + 0.1% isopropylamine) to give **5** as the first eluting isomer ($t_R = 11.2$ min). 1H NMR (400 MHz, $DMSO-d_6$): δ 8.26 (s, 1 H), 7.96 (s, 1 H), 7.65–7.76 (m, 1 H), 7.55–7.63 (m, 1 H), 7.41–7.52 (m, 3 H), 7.29–7.38 (m, 2 H), 7.19 (bs, 2 H), 5.25–5.43 (m, 1 H), 2.72 (s, 3 H), 1.89 (s, 3 H), 1.78 (d, $J = 7.06$ Hz, 3 H).

(*aS,R*)-2-[(6-Amino-9H-purin-9-yl)methyl]-5-methyl-3-phenylquinazolin-4(3H)-one (**6**). Mixture of diastereoisomers **13** was separated by chiral HPLC on a Chiralpak IC under isocratic elution at 0.8 mL/min (phase A/B = 65/35% v/v; phase A, hexane; phase B, EtOH + 0.1% isopropylamine), giving **6** as the second eluting isomer ($t_R = 12.6$ min). 1H NMR (400 MHz, $DMSO-d_6$): δ 8.16 (s, 1 H), 7.94 (s, 1 H), 7.60–7.77 (m, 1 H), 7.42–7.54 (m, 2 H), 7.26–7.38 (m, 2 H), 7.16 (bs, 2 H), 7.03–7.09 (m, 1 H), 6.73–7.01 (m, 1 H), 5.15–5.39 (m, 1 H), 2.69 (s, 3 H), 2.10 (s, 3 H), 1.64 (d, $J = 6.62$ Hz, 3 H).

(*aR,S*)-2-[(6-Amino-9H-purin-9-yl)methyl]-5-methyl-3-phenylquinazolin-4(3H)-one (**7**). Isomer **7** coeluted with **8** with the first chiral chromatography employed to isolate **5** and **6**. The title compound was thus isolated with another chiral HPLC on Chiralpak AD-H under isocratic elution at 0.8 mL/min (phase A/B = 60/40% v/v; phase A, hexane; phase B, EtOH + 0.1% isopropylamine) which gave compound **7** as first eluting isomer (rt 9.4 min). 1H NMR (400 MHz, $DMSO-d_6$): δ 8.26 (s, 1 H), 7.96 (s, 1 H), 7.65–7.75 (m, 1 H), 7.53–7.63 (m, 1 H), 7.39–7.51 (m, 3 H), 7.28–7.38 (m, 2 H), 7.19 (bs, 2 H), 5.21–5.45 (m, 1 H), 2.72 (s, 3 H), 1.89 (s, 3 H), 1.78 (d, $J = 7.06$ Hz, 3 H).

(*aR,R*)-2-[(6-Amino-9H-purin-9-yl)methyl]-5-methyl-3-phenylquinazolin-4(3H)-one (**8**). Compound **8** was separated from **7** under chiral HPLC on Chiralpak AD-H under isocratic elution at 0.8 mL/min (phase A/B = 60/40% v/v; phase A, hexane; phase B, EtOH + 0.1% isopropylamine). Compound **8** was identified as second eluting isomer compound **8** ($t_R = 16.4$ min). 1H NMR (400 MHz, $DMSO-d_6$): δ 8.19 (s, 1 H), 7.98 (s, 1 H), 7.62–7.75 (m, 1 H), 7.42–7.56 (m, 2 H), 7.31–7.40 (m, 2 H), 7.19 (bs, 2 H), 7.05–7.13 (m, 1 H), 6.93–

7.04 (m, 1 H), 5.19–5.47 (m, 1 H), 2.73 (s, 3 H), 2.13 (s, 3 H), 1.59–1.74 (m, 3 H).

2-Amino-6-methyl-*N*-phenylbenzamide (**10a**). Thionyl chloride (0.290 mL, 3.97 mmol) was added to a stirred solution of 2-amino-6-methylbenzoic acid (0.2 g, 1.32 mmol) in toluene (20 mL), and the mixture was refluxed for 18 h. The reaction was then cooled to room temperature, and the solvent was removed under reduced pressure and stripped down twice with toluene (25 mL). The residue was dissolved in DCM (20 mL) and reacted with TEA (0.277 mL, 1.98 mmol) and aniline (0.181 mL, 1.98 mmol). The slurry was then refluxed for 2 h. The reaction mixture was purified with a silica gel cartridge eluting with DCM to give the title compound **10a** (0.120 g, 0.53 mmol, 40% yield) as colorless solid. MS (ESI): 330–332 $[M + H]^+$. 1H NMR ($CDCl_3$): δ 3.42 (s, 3 H), 3.49 (s, 3 H), 4.11 (s, 3 H), 6.19 (s, 1 H), 6.90 (d, 1 H, $J = 16.2$ Hz), 7.08 (d, 1 H, $J = 16.2$ Hz), 7.29–7.37 (m, 3 H), 7.50 (s, 1 H). ^{13}C NMR ($CDCl_3$): δ 27.9, 31.7, 31.8, 90.9, 111.4, 116.1, 124.9, 126.3, 128.5, 130.1, 131.4, 134.9, 135.6, 138.1, 139.5, 151.5, 155.8. FTIR (Nujol, cm^{-1}): 1647, 1685, 2854, 2924. Mp: 200 °C.

2-Amino-6-methyl-*N*-*o*-tolylbenzamide (**10b**). Thionyl chloride (0.579 mL, 7.94 mmol) was added to a stirred solution of 2-amino-6-methylbenzoic acid (0.4 g, 2.65 mmol) in toluene (30 mL), and the mixture was refluxed for 18 h. The reaction was then cooled to room temperature, and the solvent was removed under reduced pressure and stripped down twice with toluene. The residue was dissolved in DCM (30 mL) and reacted with TEA (0.553 mL, 3.97 mmol) and *o*-toluidine (0.424 mL, 3.97 mmol). The slurry was then refluxed for 2 h. The reaction mixture was purified by silica gel flash chromatography, eluting with a gradient of petroleum ether and EtOAc to give the title compound **10b** (0.278 g, 1.16 mmol, 44% yield) as pale yellow gum. MS (ESI): $[M + H]^+ 241.4$. 1H NMR (300 MHz, $CDCl_3$): δ 2.29 (s, 3 H); 2.44 (s, 3 H); 4.16 (bs, 2 H); 6.53–6.56 (d, 1 H); 6.62–6.64 (s, 1 H); 7.06–7.11 (t, 1 H); 7.13–7.18 (t, 1 H); 7.23–7.26 (m, 2 H); 7.65 (bs, 1 H); 7.84–7.87 (s, 1 H). ^{13}C NMR (75.5 MHz, $CDCl_3$): δ 18.16; 20.34; 114.08; 120.37; 122.98; 123.71; 125.75; 126.76; 130.15; 130.27; 130.72; 135.41; 135.47; 144.97; 167.92.

2-(Chloroethyl)-5-methyl-3-phenylquinazolin-4(3H)-one (**12a**). 2-Amino-6-methyl-*N*-phenylbenzamide **10a** (0.120 g, 0.53 mmol) was dissolved in AcOH (5 mL) and reacted with 2-chloroacetyl chloride **11a** (0.084 mL, 1.06 mmol), and the mixture was refluxed for 18 h. The reaction was then cooled and concentrated under reduced pressure, and the residue was straightforward purified by silica gel flash chromatography with a gradient of petroleum ether and AcOEt to give the title compound **12a** (0.052 g, 0.183 mmol, 34% yield). MS (ESI): $[M + H]^+ 285.2$. 1H NMR (300 MHz, $CDCl_3$): δ 2.86 (s, 3 H); 4.26 (s, 2 H); 7.31–7.33 (dd, 1 H); 7.33–7.40 (m, 2 H); 7.56–7.70 (m, 5 H). ^{13}C NMR (75.5 MHz, $CDCl_3$): δ 23.01; 43.56; 120.11; 125.97; 128.85 (2 C); 129.69; 129.87 (2 C); 130.64; 133.95; 136.21; 141.76; 148.59; 151.18; 162.66.

2-(1-Chloroethyl)-5-methyl-3-*o*-tolylquinazolin-4(3H)-one (**12b**). 2-Amino-6-methyl-*N*-*o*-tolylbenzamide **10b** (0.278 g, 1.16 mmol) was dissolved in AcOH (10 mL) and reacted with 2-chloropropanoyl chloride **11b** (0.225 mL, 2.31 mmol) and the mixture refluxed for 18 h. The reaction was cooled and concentrated under reduced pressure and the residue was straightforward purified by silica gel flash chromatography with a gradient of petroleum ether and AcOEt to give the title compound **12b** (0.082 g, 0.262 mmol, 23% yield) as yellow gum. MS (ESI): $[M + H]^+ 313.2$. 1H NMR (400 MHz, $CDCl_3$): δ 1.87–1.88 (d, 3 H); 1.90–1.91 (d, 3 H); 2.09 (s, 3 H); 2.29 (s, 3 H); 2.87 (s, 6 H); 4.34–4.39 (q, 1 H); 4.65–4.70 (q, 1 H); 7.09–7.11 (d, 1 H); 7.31–7.32 (d, 2 H); 7.36–7.49 (m, 7 H); 7.65–7.70 (m, 4 H). ^{13}C NMR (100.6 MHz, $CDCl_3$): δ 17.65; 18.10; 22.28; 22.53; 23.03; 23.06; 52.45; 52.57; 119.64; 119.91; 126.16; 126.21; 127.33; 127.59; 127.92; 129.67; 129.79; 129.86; 130.34; 131.17; 131.89; 133.76; 135.20; 135.27; 135.54; 137.49; 141.73; 148.78; 148.81; 154.06; 154.23; 161.92; 162.19.

2-[(6-Amino-9H-purin-9-yl)methyl]-5-methyl-3-phenylquinazolin-4(3H)-one (**13**). 2-(1-Chloroethyl)-5-methyl-3-*o*-tolylquinazolin-4(3H)-one **12b** (0.057 g, 0.182 mmol) was dissolved in acetonitrile (15 mL) with few drops of DMF. K_2CO_3 (0.038 g, 0.273 mmol) and

adenine (0.037 g, 0.273 mmol) were added, and the mixture was reacted at 65 °C for 24 h. Solvent was then removed, and the reaction was taken up with DMF (10 mL), and then the mixture was heated under microwave irradiation at 130 °C for 4 h. The crude was directly purified by preparative HPLC (Shimadzu, neutral phase) to give the title compound **13** (0.020 g, 0.049 mmol, 27% yield).

NMR Characterization of Compound 1 and 1:R-Pirkle Complex. *Compound 1.* The title compound was dissolved in 0.75 mL of CDCl₃ 99.96% at room temperature. The obtained solution was transferred into an NMR tube and taken to the NMR analysis. Complete characterization was run in CDCl₃ 99.96%. Compound **1** (CDCl₃): ¹H NMR (400 MHz, chloroform-*d*) δ 8.26 (s, 1H), 7.89 (s, 1H), 7.54–7.63 (m, 1H), 7.45 (d, *J* = 4.41 Hz, 2H), 7.33–7.42 (m, 2H), 7.26 (m, 1H), 7.21 (d, *J* = 7.50 Hz, 1H), 5.66 (br s, 2H), 4.75–5.18 (m, 2H), 2.83 (s, 3H), 2.22 (s, 3H).

Association Complex. Compound **1** (1 mg, 2.5 × 10⁻³ mmol) was dissolved in 0.75 mL of CDCl₃ 99.96% at rt, and this solution was added to chiral reagent (1R)-1-(anthracen-9-yl)-2,2,2-trifluoroethanol (*R*-Pirkle, 6.9 mg, 25 × 10⁻³ mmol, molar ratio 1:10 with respect to the standard). The mixture was transferred into an NMR tube and taken to the NMR analysis. Compound 1:*R*-Pirkle (CDCl₃): ¹H NMR (400 MHz, chloroform-*d*) δ 8.97 (br s, 9H), 8.53 (s, 11H), 7.89–8.27 (m, 31H), 7.44–7.69 (m, 44H), 7.29–7.40 (m, 3H), 7.24–7.26 (m, 2H), 6.89–7.12 (m, 1H), 6.65 (q, *J* = 7.83 Hz, 10H), 5.49 (br s, 2H), 4.42–4.99 (m, 2H), 3.36 (br s, 10H), 2.81 (d, *J* = 7.83 Hz, 3H), 2.11 (d, *J* = 14.09 Hz, 3H).

Stability Study. Compound **2** and compound **3** were dissolved in dimethyl sulfoxide (DMSO) at 5 mg/mL (10 mM) and 0.5 mg/mL (1 mM) and stored at two different temperatures, i.e., 37 and -20 °C for 9 weeks. Samples were diluted to 1 μg/mL with methanol before injection. The stability of both solutions was evaluated by HPLC/MS using a Acquity UPLC system (Waters) coupled with a 5500-QTrap MS instrument (AB Sciex) equipped with an ESI source. A column Lux Cellulose-1, 5 μm, 4.6 mm × 250 mm, was employed at 30 °C. Solutions used as eluent: HCOONH₄ 0.025 M, pH 3 (A); ACN/MeOH 40/60 (B) (isocratic, 35% A, 65% B). The injection volume was 5 μL, the flow was 0.6 mL/min, while the run time was 18 min. All the MS data were acquired in positive-ion mode applying the multiple-reaction-monitoring (MRM) settings.

Molecular Modeling. Potential Energy Barrier Estimation by DFT. Quantum chemical calculations were performed using the Jaguar 7.8³⁸ within Maestro suite 9.2.³⁹ In Jaguar, relaxed torsion scans of the dihedral angle N–C1–C2–C3 of the model compound were defined for a range of 180° at 15° intervals, starting from the value of 90°. In the vicinity of the approximate transition state (at 0°) additional angle values were collected (i.e., ±10° and ±5°). At each restrained torsion angle, the geometry was optimized by using the hybrid functional B3LYP in combination with B3LYP/6-31G* basis set. SCF and convergence criteria were set at 5.0 × 10⁻⁵ hartrees or rms density matrix change of 5.0 × 10⁻⁵ hartrees, whichever was satisfied first.

Model Building and Application of a QM/MM Potential. Compound **2** was taken from the coordinate of 2X38.pdb and imported into Maestro 9.2.³⁴ Atom types and bond orders were corrected, and hydrogen atoms were added. The resulting structure was immersed in a box of TIP3P water molecules (1397 residues) using the Xleap tool of AMBER 10.⁴⁰ The total system size amounted to 4240 atoms (box size of 37.1 Å × 41.0 Å × 39.6 Å). The system was minimized using the AMBER99SB force field,⁴¹ in the SANDER module of AMBER 10 and then used for QM/MM calculations. The 2–TIP3P system was thermalized (300 K) in the NVT ensemble for 100 ps using the QM/MM scheme implemented in the SANDER module of the AMBER 10 suite. All the atoms of **2** (49 in total) were treated with the self-consistent charge-density functional tight-binding (SCC-DFTB) approach, as implemented in SANDER. The solvent atoms were described with AMBER99SB force field. During QM/MM MD simulations (either plain or biased), all the atoms of the system (including hydrogens) were free to move, and a time step of 0.2 fs was used to integrate the equation of motion.

Umbrella Sampling Simulations. Starting from the equilibrated 2–TIP3P system, an umbrella sampling calculation was performed by

imposing constraining potentials along the ϕ dihedral angle of **2** (Figure 4), with a force constant of 500 kcal mol⁻¹ Å⁻² from the value of 90° up to -90°. In this way, the ortho methyl group of **2** was gradually moved from one side of the plane identified by the quinazolin-4-one nucleus to the other. The interval between each harmonic potential was 10° for a total of 19 simulation windows. The sampling for each harmonic potential consisted of 200 ps, for a total of 3.8 ns of QM/MM simulation. We discarded the statistics from the first 100 ps to allow a suitable relaxation from the imposed bias. The final free energy profile was obtained by using the weighted histogram analysis method (WHAM)⁴² on the collected statistics.

High-Level Correction. The geometries of the starting structure and of the approximate TS from SCC-DFTB/AMBER simulations were isolated, and gas-phase energy calculations were performed at the SCC-DFTB and B3LYP/6-31G* levels. The corrected energies were calculated applying the computational protocol described in ref 43. In brief the revised energies were obtained by subtracting from the total QM/MM energy the SCC-DFTB energy of the isolated QM region and adding the B3LYP energy. The B3LYP corrected free energies therefore consist of the B3LYP vacuum energy, of the AMBER MM energy, and of the SCC-DFTB/AMBER99 QM/MM interaction energy.

Conformational Analysis by wt-Metadynamics. *wt-META-D* simulations were conducted with Desmond version 3.0.⁴⁴ The dihedral angles χ₁ and χ₂ reported in Figure 4 were used as collective variables (CVs) to sample the conformational space of compounds **2** and **5–8**. Compounds **5–8** were built using the sketching tool of Maestro. The geometry of the compounds was optimized using OPLS2005 force field in combination with GB/SA water model. Then, the compounds were placed into a cubic box of TIP3P water molecules,⁴⁵ leaving a minimum distance of 24 Å between any ligand atom and the edges of the box. The solvated systems were first relaxed using two energy minimization processes, aimed at relieving major steric clashes. While in the first minimization stage all solute heavy atoms were constrained with a force constant of 50 kcal mol⁻¹ Å⁻² and the convergence threshold was set to 50 kcal mol⁻¹, in the second minimization step the threshold was decreased to 5 kcal mol⁻¹ and all constraints were removed. A plain MD simulation was then performed to relax each system before the META-D run. The relaxation phase comprised (i) 100 ps in the NVT ensemble at 10 K with a constraint of 50 kcal/(mol·Å²) on solute heavy atoms, (ii) 100 ps in the NPT ensemble at 10 K with a constraint of 50 kcal/(mol·Å²) on solute heavy atoms, (iii) 100 ps in the NPT ensemble at 300 K with a constraint of 50 kcal/(mol·Å²) on solute heavy atoms, (iv) 200 ps in the NPT ensemble at 300 K without constraints. META-D simulations were conducted in the NPT ensemble at 300 K and 1 atm for 50 ns, applying the Langevin thermostat and barostat. The M-SHAKE⁴⁶ was used to constrain all bond lengths to hydrogen atoms. Long-range electrostatic interactions were computed using the smooth particle mesh Ewald method,⁴⁷ whereas short-range electrostatic interactions were cut off at 9 Å. A RESPA integrator⁴⁸ was used to compute the bonded, van der Waals, and short-range electrostatic interactions every 2 fs, whereas long-range electrostatics were computed every 6 fs. Gaussian potentials were added every 0.09 ps with a height of 0.03 kcal/mol and a width of 5°. The OPLS2005 force field was used in all calculations. FESs were then reconstructed from the Gaussian potentials using the Desmond metadynamics analysis tool implemented in Maestro 9.2. The convergence of *wt-META-D* simulations was assessed by evaluating the time evolution of the relative free-energy levels of the key free-energy minima. To this end, *wt-META-D* were run for 50 ns, while FESs were reconstructed at every nanosecond of simulation. The simulations were considered at convergence when the free-energy difference among global and local minima became approximately constant. For the compounds **2** and **5–8**, simulations converged approximately after 30 ns (see Supporting Information Figures S3–S7). The FESs reported in Figure 6 are those reconstructed at the end of the simulations.

Conformational Energies by DFT Calculations. OPLS-2005 minima identified on the FES of Figure 6 for compounds **2**, **5**, and **6** were used as input structures for DFT optimization in implicit

solvent (PCM, water) at M06-2X/6-31G**/PCM = H₂O level. Solvation energies were calculated using the Poisson–Boltzmann equation solver implemented in Jaguar.⁴⁹ The resulting geometries were used as input structures for single point calculation at M06-2X/cc-PVTZ(-f)/PCM = H₂O level. Default convergence criteria for SCF calculation and geometry optimization were applied.

Vibrational Circular Dichroism (VCD) Studies. The absolute configuration of each atropisomer of compound 1 (i.e., compounds 2 and 3) as well as of compounds 5–8 was determined recording VCD spectra in tandem with calculations of the predicted spectra.⁵⁰ In brief, the experimental VCD spectra of the inhibitors were recorded on a BioTools/Bomem Dual PEM chiral IR spectrometer (Biotoools, Inc., Jupiter, FL) using a 100 μ m liquid cell equipped with BaF₂ windows. Spectra were recorded using CDCl₃ as solvent. For all samples, 40 000 scans were recorded at 4 cm⁻¹ resolution and averaged, while the spectrum obtained for the pure solvent was used for solvent subtraction. Concentrations of 5 mg in 150 μ L were used. A systematic conformational analysis of 2–8 was carried out using the MMFF94 molecular mechanics force⁵¹ field implemented in Sybyl-X software.⁵² For each compound, potential energy minima obtained were optimized using DFT at wB97XD/cc-pvtz level using a PCM continuum model for solvent representation (chloroform). Boltzmann weighted VCD spectra were then calculated using Gaussian 09 program⁵³ at the same level of theory. Comparison of the DFT calculated spectra to the experimental ones enables the absolute configuration of 2, 3, and 5–8 to be reliably determined.^{54,55}

Biological Test Methods. In Vitro Kinase Assay. Human recombinant PI3K δ was purchased from Millipore Ltd. (Billerica, MA). Compounds were dissolved at 0.5 mM in DMSO and were tested at different concentrations for their activity against PI3K δ using the ADP-Glo kinase assay (Promega, Madison, WI) according to the manufacturer's instructions. Briefly, the kinase reactions were performed in 384-well white plates (Greiner Bio-One GmbH, Frickenhausen). Each well was loaded with 0.1 μ L of test compounds and 2.5 μ L of 2 \times reaction buffer (40 mM Tris, pH 7.5, 0.5 mM EGTA, 0.5 mM Na₃VO₄, 5 mM β -glycerophosphate, 0.1 mg/mL BSA, 1 mM DTT), containing 50 μ M PI and PS substrates (*L*- α -phosphatidylinositol sodium salt and *L*- α -phosphatidyl-L-serine, Sigma-Aldrich, St. Louis, MO) and the PI3K recombinant protein (PI3K δ 1 ng/ μ L). The reactions were started by adding 2.5 μ L of 2 \times ATP solution to each well (final concentration ATP 80 μ M) and incubated for 60 min at room temperature. Subsequently, each kinase reaction was incubated for 40 min with 5 μ L of ADP-Glo reagent, allowing depletion of unconsumed ATP. Then, the kinase detection reagent (10 μ L) was added in each well to convert ADP to ATP and to allow the newly synthesized ATP to be measured using a luciferase/luciferin reaction. Following a 60 min incubation, the luminescence signal was measured using a Wallac EnVision multilabel reader (PerkinElmer, Waltham, MA). Curve fitting and pIC₅₀ calculation were carried out using a four-parameter logistic model in XLfit (IDBS, Guilford, U.K.) for Microsoft Excel (Microsoft, Redmont, WA).

Determination of PI3K Inhibitory Activity in the PBMCs Assay. Human peripheral blood mononuclear cells (PBMCs) were purchased from Lonza (Basel, CH), washed, and resuspended in RPMI 1640 medium (without phenol red) supplemented with 10% FBS, 2 mM glutamine, 100 U/mL penicillin, and 100 μ g/mL streptomycin (Thermo Fisher Scientific, Waltham, MA). PBMCs were plated at a density of 10⁵ cells/well in 96-well plates coated with 6 μ g/mL anti-human CD3 antibody (Biologend, San Diego, CA). Cells were treated in RPMI 1640 medium (without phenol red) supplemented with 10% FBS with different concentrations of PI3K inhibitors (10⁻¹²–10⁻⁵ M, final DMSO concentration 0.2%), co-stimulated with 3 μ g/mL anti-human CD28 antibody (BD Biosciences, San Jose, CA), and incubated for 72 h in an atmosphere of 95% air and 5% CO₂ at 37 °C. Human IL-6 was measured in the supernatants using paired antibody quantitative ELISA kit (from Thermo Fisher Scientific, Waltham, MA) according to the manufacturer's instructions. pIC₅₀ values were determined from concentration–response curves by nonlinear regression analysis using Graph Pad Prism, version 6 (GraphPad Software, La Jolla, CA).

■ ASSOCIATED CONTENT

📄 Supporting Information

The Supporting Information is available free of charge on the ACS Publications website at DOI: 10.1021/acs.jmedchem.7b00247.

Molecular formula strings and some data for compounds 2–8 (CSV)

¹H NMR spectrum (CDCl₃, 25 °C) of compound 1 alone or in complex with R-Pirkle; plots reporting time evolution of the free-energy differences among key minima identified on conformational FES reconstructed by *wt*-META-D for compounds 2, 5–8; M06-2X/cc-PVTZ(-f) energies for compounds 2, 5, and 6; experimental details for the HPLC-based stability studies performed on compounds 2 and 3 (PDF)

■ AUTHOR INFORMATION

Corresponding Authors

*M.M.: phone, +39 0521 905059; fax, + 39 0521 905006; e-mail, marco.mor@unipr.it.

*A.M.C.: phone, +39 0521 279188; fax, + 39 0521 279880; e-mail, am.capelli@chiesi.com.

ORCID

Alessio Lodola: 0000-0002-8675-1002

Marco Mor: 0000-0003-0199-1849

Daniele Pala: 0000-0001-6160-6127

Silvia Rivara: 0000-0001-8058-4250

Present Address

^{||}D.P.: Chiesi Farmaceutici S.p.A., Largo Belloli, 11/A, Parma, Italy.

Author Contributions

The manuscript was written through contributions of all authors. All authors have given approval to the final version of the manuscript.

Notes

The authors declare no competing financial interest.

■ ABBREVIATIONS USED

PI3K, phosphoinositide 3-kinase; IL-6, interleukin-6; DFT, density functional theory; FES, free-energy surface; *wt*-META-D, well-tempered metadynamics; PBMC, peripheral blood mononuclear cell; VCD, vibrational circular dichroism

■ REFERENCES

- (1) Oki, M. Recent Advances in Atropisomerism. In *Topics in Stereochemistry*; Allinger, N. L., Eliel, N. L., Wilen, S. H., Eds.; John Wiley & Sons: New York, 1983; Vol. 14, pp 1– 81, DOI: 10.1002/9780470147238.ch1.
- (2) Eichelbaum, M.; Gross, A. S. Stereochemical aspects of drug action and disposition. *Adv. Drug Res.* 1996, 28, 1–6.
- (3) Clayden, J.; Moran, W. J.; Edwards, P. J.; LaPlante, S. R. The challenge of atropisomerism in drug discovery. *Angew. Chem., Int. Ed.* 2009, 48, 6398–6401.
- (4) LaPlante, S. R.; Forgione, P.; Boucher, C.; Coulombe, R.; Gillard, J.; Hucce, O.; Jakalian, A.; Joly, M.-A.; Kukulj, G.; Lemke, C.; McCollum, R.; Titolo, S.; Beaulieu, P. L.; Stammers, T. Enantiomeric atropisomers inhibit HCV polymerase and/or HIV matrix: characterizing hindered bond rotations and target selectivity. *J. Med. Chem.* 2014, 57, 1944–1951.
- (5) Webster, R.; Cole, S.; Gedge, J.; Roffey, S.; Walker, D.; Wild, W. Pharmacokinetics and disposition of a novel NMDA glycine site

- antagonist (UK-240,455) in rats, dogs and man. *Xenobiotica* **2003**, *33*, 541–560.
- (6) Elleraas, J.; Ewanicki, J.; Johnson, T. W.; Sach, N. W.; Collins, M. R.; Richardson, P. F. Conformational studies and atropisomerism kinetics of the ALK clinical candidate lorlatinib (PF-06463922) and desmethyl congeners. *Angew. Chem., Int. Ed.* **2016**, *55*, 3590–3595.
- (7) Glunz, W. P.; Mueller, L.; Cheney, L. D.; Ladziata, V.; Zou, Y.; Wurtz, N. R.; Wei, A.; Wong, P.; Wexler, R. R.; Priestley, E. S. Atropisomer control in macrocyclic factor VIIa inhibitors. *J. Med. Chem.* **2016**, *59*, 4007–4018.
- (8) LaPlante, S. R.; Fader, L. D.; Fandrick, K. R.; Fandrick, D. R.; Hucke, O.; Kemper, R.; Miller, S. P. F.; Edwards, P. J. Assessing atropisomer axial chirality in drug discovery and development. *J. Med. Chem.* **2011**, *54*, 7005–7022.
- (9) LaPlante, S. R.; Edwards, P. J.; Fader, L. D.; Jakalian, A.; Hucke, O. Revealing atropisomer axial chirality in drug discovery. *ChemMedChem* **2011**, *6*, 505–513.
- (10) Xing, L.; Devadas, B.; Devraj, R. V.; Selness, S. R.; Shieh, H.; Walker, J. K.; Mao, M.; Messing, D.; Samas, B.; Yang, J. Z.; Anderson, G. D.; Webb, E. G.; Monahan, J. B. Discovery and characterization of atropisomer PH-797804, a p38 MAP kinase inhibitor, as a clinical drug candidate. *ChemMedChem* **2012**, *7*, 273–280.
- (11) Sadhu, C.; Masinovsky, B.; Dick, K.; Sowell, C. G.; Staunton, D. E. Essential role of phosphoinositide 3-kinase delta in neutrophil directional movement. *J. Immunol.* **2003**, *170*, 2647–2654.
- (12) Everts, J. B.; Ulrich, R. G. Atropoisomers of 2-Purinylyl-3-tolylquinazolinone derivatives and methods of use. WO 2010/111432, 2010.
- (13) Marahatta, A.; Bhandary, B.; Lee, Y. C.; Kim, S. R.; Chae, H.-J. Development and validation of a highly sensitive LC-MS/MS method for quantification of IC87114 in mice plasma, bronchoalveolar lavage and lung samples: Application to pharmacokinetic study. *J. Pharm. Biomed. Anal.* **2014**, *89*, 197–202.
- (14) Thappali, S. R.; Varanasi, K. V.; Veeraraghavan, S.; Vakkalanka, S. K.; Mukkanti, K. Simultaneous quantitation of IC87114, Roflumilast and its active metabolite Roflumilast N-oxide in plasma by LC-MS/MS: application for a pharmacokinetic study. *J. Mass Spectrom.* **2012**, *47*, 1612–1619.
- (15) Spadoni, G.; Bedini, A.; Lucarini, S.; Mari, M.; Caignard, D. H.; Boutin, J. A.; Delagrèze, P.; Lucini, V.; Scaglione, F.; Lodola, A.; Zanardi, F.; Pala, D.; Mor, M.; Rivara, S. Highly potent and selective MT2 melatonin receptor full agonists from conformational analysis of 1-benzyl-2-acylaminoethyl-tetrahydroquinolines. *J. Med. Chem.* **2015**, *58*, 7512–7525.
- (16) Bedini, A.; Lucarini, S.; Spadoni, G.; Tarzia, G.; Scaglione, F.; Dugnani, S.; Pannacci, M.; Lucini, V.; Carmi, C.; Pala, D.; Rivara, S.; Mor, M. Toward the definition of stereochemical requirements for MT2-selective antagonists and partial agonists by studying 4-phenyl-2-propionamidotetralin derivatives. *J. Med. Chem.* **2011**, *54*, 8362–8372.
- (17) Berndt, A.; Miller, S.; Williams, O.; Le, D. D.; Houseman, B. T.; Pacold, J. I.; Gorrec, F.; Hon, W.-C.; Liu, Y.; Rommel, C.; Gaillard, P.; Rückle, T.; Schwarz, M. K.; Shokat, K. M.; Shaw, J. P.; Williams, R. L. The p110 δ crystal structure: mechanisms for selectivity and potency of new PI(3)K inhibitors. *Nat. Chem. Biol.* **2010**, *6*, 117–124.
- (18) Avey-David, H. H.; Senderowitz, H. Toward focusing conformational ensembles on bioactive conformations: a molecular mechanics/quantum mechanics study. *J. Chem. Inf. Model.* **2015**, *55*, 2154–2167.
- (19) Stephens, P. J.; Devlin, F. J.; Chabalowski, C. F.; Frisch, M. J. *Ab Initio* calculation of vibrational absorption and circular dichroism spectra using density functional force fields. *J. Phys. Chem.* **1994**, *98*, 11623–11627.
- (20) (a) Warshel, A.; Levitt, M. Theoretical studies of enzymic reactions: dielectric, electrostatic and steric stabilization of the carbonium ion in the reaction of lysozyme. *J. Mol. Biol.* **1976**, *103*, 227–249. (b) Field, M. J.; Bash, P. A.; Karplus, M. A combined quantum mechanical and molecular mechanical potential for molecular dynamics simulations. *J. Comput. Chem.* **1990**, *11*, 700–733.
- (c) Lodola, A.; De Vivo, M. The increasing role of QM/MM in drug discovery. *Adv. Protein Chem. Struct. Biol.* **2012**, *87*, 337–362.
- (21) Madarász, Á.; Berta, D.; Paton, R. S. Development of a true transition state force field from quantum mechanical calculations. *J. Chem. Theory Comput.* **2016**, *12*, 1833–1844.
- (22) Carloni, P.; Alber, F. Quantum medicinal chemistry. In *Methods and Principles in Medicinal Chemistry*; Mannhold, R., Kubinyi, H., Folkers, G., Eds.; Wiley-VCH: Weinheim, Germany, 2003.
- (23) (a) Becke, A. D. Density-functional thermochemistry. III. The role of exact exchange. *J. Chem. Phys.* **1993**, *98*, 5648–5652. (b) Becke, A. D. A new mixing of Hartree-Fock and local density-functional theories. *J. Chem. Phys.* **1993**, *98*, 1372–1377. (c) Lee, C. T.; Yang, W. T.; Parr, R. G. Development of the Colle-Salvetti correlation-energy formula into a functional of the electron-density. *Phys. Rev. B: Condens. Matter Mater. Phys.* **1988**, *37*, 785–789.
- (24) Elstner, M. The SCC-DFTB method and its application to biological systems. *Theor. Chem. Acc.* **2006**, *116*, 316–325.
- (25) Walker, R. C.; Crowley, M. F.; Case, D. A. The implementation of a fast and accurate QM/MM potential method in AMBER. *J. Comput. Chem.* **2008**, *29*, 1019–1031.
- (26) Rajamani, R.; Naidoo, K. J.; Gao, J. Implementation of an adaptive umbrella sampling method for the calculation of multidimensional potential of mean force of chemical reactions in solution. *J. Comput. Chem.* **2003**, *24*, 1775–1781.
- (27) Patel, L.; Chandrasekhar, J.; Everts, J.; Forseth, K.; Haran, A. C.; Ip, C.; Kashishian, A.; Kim, M.; Koditek, D.; Koppenol, S.; Lad, L.; Lepist, E. I.; McGrath, M. E.; Perreault, S.; Puri, K. D.; Villaseñor, A. G.; Somoza, J. R.; Steiner, B. H.; Therrien, J.; Treiber, J.; Phillips, G. Discovery of orally efficacious phosphoinositide 3-kinase δ inhibitors with improved metabolic stability. *J. Med. Chem.* **2016**, *59*, 9228–9242.
- (28) Eyring, H. The activated complex in chemical reactions. *J. Chem. Phys.* **1935**, *3*, 107–115.
- (29) Barducci, A.; Bussi, G.; Parrinello, M. Well-tempered metadynamics: a smoothly converging and tunable free-energy method. *Phys. Rev. Lett.* **2008**, *100*, 020603.
- (30) Kaminski, G. A.; Friesner, R. A.; Tirado-Rives, J.; Jorgensen, W. L. Evaluation and reparametrization of the OPLS-AA force field for proteins via comparison with accurate quantum mechanical calculations on peptides. *J. Phys. Chem. B* **2001**, *105*, 6474–6487.
- (31) De Vivo, M.; Masetti, M.; Bottegoni, G.; Cavalli, A. Role of molecular dynamics and related methods in drug discovery. *J. Med. Chem.* **2016**, *59*, 4035–4061.
- (32) Vymetal, J.; Vondrášek, J. Metadynamics as a tool for mapping the conformational and free-energy space of peptides - The alanine dipeptide case study. *J. Phys. Chem. B* **2010**, *114*, 5632–5642.
- (33) Laio, A.; Parrinello, M. Escaping free-energy minima. *Proc. Natl. Acad. Sci. U. S. A.* **2002**, *99*, 12562–12566.
- (34) (a) Laio, A.; Gervasio, F. L. Metadynamics: a method to simulate rare events and reconstruct the free energy in biophysics, chemistry and material science. *Rep. Prog. Phys.* **2008**, *71*, 126601. (b) Scalvini, L.; Vacondio, F.; Bassi, M.; Pala, D.; Lodola, A.; Rivara, S.; Jung, K. M.; Piomelli, D.; Mor, M. Free-energy studies reveal a possible mechanism for oxidation-dependent inhibition of MGL. *Sci. Rep.* **2016**, *6*, 31046. (c) Russo, S.; Callegari, D.; Incerti, M.; Pala, D.; Giorgio, C.; Brunetti, J.; Bracci, L.; Vicini, P.; Barocelli, E.; Capoferri, L.; Rivara, S.; Tognolini, M.; Mor, M.; Lodola, A. Exploiting free-energy minima to design novel EphA2 protein-protein antagonists: from simulation to experiment and return. *Chem. - Eur. J.* **2016**, *22*, 8048–8052.
- (35) Callegari, D.; Lodola, A.; Pala, D.; Rivara, S.; Mor, M.; Rizzi, A.; Capelli, A. M. Metadynamics simulations distinguish short- and long-residence-time inhibitors of cyclin-dependent kinase 8. *J. Chem. Inf. Model.* **2017**, *57*, 159–169.
- (36) Hohenstein, E. G.; Chill, S. T.; Sherrill, C. D. Assessment of the performance of the M05-2X and M06-2X exchange-correlation functionals for noncovalent interactions in biomolecules. *J. Chem. Theory Comput.* **2008**, *4*, 1996–2000.
- (37) Ge, Q.; Moir, L. M.; Trian, T.; Niimi, K.; Poniris, M.; Shepherd, P. R.; Black, J. L.; Oliver, B. G.; Burgess, J. K. The phosphoinositide 3-

kinase p110 δ modulates contractile protein production and IL-6 release in human airway smooth muscle. *J. Cell. Physiol.* **2012**, *227*, 3044–3052.

- (38) *Jaguar*, version 7.8; Schrödinger, LLC: New York, NY, 2011.
- (39) *Maestro*, version 9.2; Schrödinger, LLC: New York, NY, 2011.
- (40) Cornell, W. D.; Cieplak, P.; Bayly, C. L.; Gould, I. R.; Merz, K. M.; Ferguson, D. M.; Spellmeyer, D. C.; Fox, T.; Caldwell, J. W.; Kollman, P. A. A second generation force field for the simulation of proteins, nucleic acids, and organic molecules. *J. Am. Chem. Soc.* **1995**, *117*, 5179–5197.
- (41) Hornak, V.; Abel, R.; Okur, A.; Strockbine, B.; Roitberg, A.; Simmerling, C. Comparison of multiple Amber force fields and development of improved protein backbone parameters. *Proteins: Struct., Funct., Genet.* **2006**, *65*, 712–725.
- (42) Kumar, S.; Bouzida, D.; Swendsen, R. H.; Kollman, P. A.; Rosenberg, J. M. The weighted histogram analysis method for free-energy calculations on biomolecules. I. The method. *J. Comput. Chem.* **1992**, *13*, 1011–1021.
- (43) Lodola, A.; Capoferri, L.; Rivara, S.; Tarzia, G.; Piomelli, D.; Mulholland, A.; Mor, M. Quantum mechanics/molecular mechanics modeling of fatty acid amide hydrolase reactivation distinguishes substrate from irreversible covalent inhibitors. *J. Med. Chem.* **2013**, *56*, 2500–2512.
- (44) *Desmond Molecular Dynamics System*, version 3.0; D. E. Shaw Research: New York, NY, 2011.
- (45) Jorgensen, W. L.; Chandrasekhar, J.; Madura, J. D.; Impey, R. W.; Klein, M. L. Comparison of simple potential functions for simulating liquid water. *J. Chem. Phys.* **1983**, *79*, 926–935.
- (46) Krautler, V.; Van Gunsteren, W. F.; Hunenberger, P. H. A fast SHAKE: Algorithm to solve distance constraint equations for small molecules in molecular dynamics simulations. *J. Comput. Chem.* **2001**, *22*, 501–508.
- (47) Darden, T.; York, D.; Pedersen, L. Particle mesh Ewald: an N – log(N) method for Ewald sums in large systems. *J. Chem. Phys.* **1993**, *98*, 10089–10092.
- (48) Tuckerman, M.; Berne, B. J.; Martyna, G. J. Reversible multiple time scale molecular dynamics. *J. Chem. Phys.* **1992**, *97*, 1990–2001.
- (49) Bochevarov, A. D.; Harder, E.; Hughes, T. F.; Greenwood, J. R.; Braden, D. A.; Philipp, D. M.; Rinaldo, D.; Halls, M. D.; Zhang, J.; Friesner, R. A. Jaguar: a high-performance quantum chemistry software program with strengths in life and materials sciences. *Int. J. Quantum Chem.* **2013**, *113*, 2110–2142.
- (50) Stephens, P. J.; Devlin, F. J.; Pan, J. J. The determination of the absolute configuration of chiral molecules using vibrational circular dichroism (VCD) spectroscopy. *Chirality* **2008**, *20*, 643–663.
- (51) Halgren, T. A. Merck molecular force field. I. Basis, form, scope, parameterization, and performance of MMFF94. *J. Comput. Chem.* **1996**, *17*, 490–519.
- (52) *SYBYL-X Molecular Modeling Package*, version 2.0; Tripos Inc.: St. Louis, MO.
- (53) Frisch, M. J.; Trucks, H. B.; Schlegel, H. B.; Scuseria, G. E.; Robb, M. A.; Cheeseman, J. R.; Scalmani, G.; Barone, V.; Mennucci, B.; Petersson, G. A.; Nakatsuji, H.; Caricato, M.; Li, X.; Hratchian, H. P.; Izmaylov, A. F.; Bloino, J.; Zheng, G.; Sonnenberg, J. L.; Hada, M.; Ehara, M.; Toyota, K.; Fukuda, R.; Hasegawa, J.; Ishida, M.; Nakajima, T.; Honda, Y.; Kitao, O.; Nakai, H.; Vreven, T.; Montgomery, J. A., Jr.; Peralta, J. E.; Ogliaro, F.; Bearpark, M.; Heyd, J. J.; Brothers, E.; Kudin, K. N.; Staroverov, V. N.; Kobayashi, R.; Normand, J.; Raghavachari, K.; Rendell, A.; Burant, J. C.; Iyengar, S. S.; Tomasi, J.; Cossi, M.; Rega, N.; Millam, N. J.; Klene, M.; Knox, J. E.; Cross, J. B.; Bakken, V.; Adamo, C.; Jaramillo, J.; Gomperts, R.; Stratmann, R. E.; Yazyev, O.; Austin, A. J.; Cammi, R.; Pomelli, C.; Ochterski, J. W.; Martin, R. L.; Morokuma, K.; Zakrzewski, V. G.; Voth, G. A.; Salvador, P.; Dannenberg, J. J.; Dapprich, S.; Daniels, A. D.; Farkas, Ö.; Foresman, J. B.; Ortiz, J. V.; Cioslowski, J.; Fox, D. J. *Gaussian 09*; Gaussian, Inc.: Wallingford, CT, 2009.
- (54) Tamayo, N. A.; Bo, Y.; Gore, V.; Ma, V.; Nishimura, N.; Tang, P.; Deng, H.; Klionsky, L.; Lehto, S. G.; Wang, W.; Youngblood, B.; Chen, J.; Correll, T. L.; Bartberger, M. D.; Gavva, N. R.; Norman, M.

H. Fused piperidines as a novel class of potent and orally available transient receptor potential melastatin type 8 (TRPM8) antagonists. *J. Med. Chem.* **2012**, *55*, 1593–1611.

- (55) Sherer, E. C.; Lee, C. H.; Shpungin, J.; Cuff, J. F.; Da, C.; Ball, R.; Bach, R.; Crespo, A.; Gong, X.; Welch, C. J. Systematic approach to conformational sampling for assigning absolute configuration using vibrational circular dichroism. *J. Med. Chem.* **2014**, *57*, 477–494.